JOURNAL OF APPLIED ELECTROCHEMISTRY **26** (1996) 1093–1102

Hydrodynamic modelling of the liquid–solid behaviour of the circulating particulate bed electrode

B. M. DWEIK, C. C. LIU, R. F. SAVINELL*

Ernest B. Yeager Center for Electrochemical Sciences, Chemical Engineering Department, Case Western Reserve University, Cleveland, OH 44106, USA

Received 31 August 1995; revised 4 March 1996

Experimental and modelling investigations of the hydrodynamics of the internal flow structure in the circulating particulate bed electrode (CPBE) are reported. The CPBE, a hybrid between an expanded packed bed and an entrained/fluidized bed, is particularly well suited for many electrochemical applications such as metal recovery and pollution treatments for metal containing effluents. This study deals with the fundamental hydrodynamics and particle dynamics of the CPBE. A mathematical model of the CPBE has been developed which successfully describes the motion of the particles and the fluid in the bed. It is shown that many of the flow characteristics of the circulating bed can be predicted using fundamental data. The validity of the proposed model was demonstrated by comparing predictions to experimental observations of several bed characteristics under various operating conditions. The conditions necessary for a stable circulating particulate bed are defined.

List of symbols

A cross-sectional area of the cell (m^2)
d_p mean particle diameter (m)
C_D experimentally determined constant calculated by Haider and Levenspiel [26]
C proportional constant in Equation 15
CR circulation rate of solids ($m^3\,s^{-1}$)
D hydraulic diameter of the vessel (m)
g gravitational constant ($kg\,m\,s^{-2}$)
G flow rate ($kg\,s^{-1}$)
H_D height of the particles inside the descending layer (m)
H_R height of the particles inside the rising layer (m)
L length (m)
n Richardson and Zaki index (–)
ΔP pressure drop ($N\,m^{-2}$)
Q inlet liquid flow rate ($m^3\,s^{-1}$)
R reaction force between the descending layer and the cell wall ($kg\,m^{-2}$)
T total bed thickness (m)
t_D descending layer thickness
t_R rising layer thickness
$\tan\phi$ coefficient of friction (–)
U_l superficial liquid velocity ($m\,s^{-1}$)
U_i a function of terminal velocity (equation 3) ($m\,s^{-1}$)
U_t particle terminal velocity ($m\,s^{-1}$)
V interstitial velocity or actual velocity ($m\,s^{-1}$)
V_1 slip velocity in the rising layer ($m\,s^{-1}$)
V_2 slip velocity in the descending layer ($m\,s^{-1}$)
W width of the bed (m)

Greek symbols
ϵ bed voidage (the fraction of the total volume which is made up of the free space between the particles and is filled with fluid) (–)
ϵ_I packed bed voidage before bed expansion (–)
θ tilt angle (radians or degrees)
ρ_s solid density ($kg\,m^{-3}$)
ρ_f fluid density ($kg\,m^{-3}$)
μ_f solution viscosity ($kg\,m\,s^{-1}$)
ϕ_s particle sphericity (–)

Subscripts
D descending layer
L(f) liquid (fluid) component
R rising layer
S solid component
L liquid component
T total depth of the bed
P particles
t terminal

1. Introduction

Here we report research results of hydrodynamic characterization of a novel electrochemical reactor called the circulating particulate bed electrode reactor (CPBE). This resembles a combination of a spouted bed or entrained/fluidized bed and an expanded packed bed. In certain cases the CPBE is considered as a special case of what is known as slot spouted bed [1]. A quantitative understanding of the hydrodynamics of the circulating particulate bed is needed for design and scale-up of an efficient device in order to optimize its performance.

High specific surface area, good mass transfer rates

* Author to whom correspondence should be addressed.

0021-891X

and other properties have led many workers to believe that three-dimensional electrodes possess many advantages over conventional parallel plate cell reactors in applications such as organic electrosynthesis [2], metal recovery and pollution treatments of water streams and effluents [3].

Coeuret [4] reviewed the use of fluidized beds to recover metals from solutions since the appearance of the particulate electrode in 1966. The concept of the circulating bed was first described in [5]. Later the CPBE cell was developed and patented as a part of an electrochemical reactor by James and coworkers [6, 7] with some modifications and improvements by others [8, 9]. There are a few references in the open literature regarding the CPBE [10–12]. In the case of copper recovery [11], Goodridge *et al.* showed that the electronic conductivity in the dispersed phase in the CPBE is much better than the fluidized bed. Goodridge and Vance [12] demonstrated several of the positive features of the CPBE cell as applied to electrowinning of zinc such as achieving high current efficiencies in acid electrolyte at high current densities.

The lack of understanding the particle and hydrodynamics of the particulate bed is one of the reasons this technology has not been introduced into commercial applications. Therefore, this work emphasizes developing a better understanding of the hydrodynamic characteristics of the CPBE.

Preliminary studies for the hydrodynamic modelling of the circulating bed are given in [13]. In this paper we report a more coherent picture of the hydrodynamics of the CPBE as a function of cell tile angle, solution flow rate, particle size and density, and solution properties. A hydrodynamic model allows one to predict basic bed characteristics, such as descending bed particle flow rate, rising layer thickness and bed porosity. More importantly, the model can be used to predict particle movement and distribution as a function of average superficial flow rate, particle size and density, fluid properties, cell tilt angle and cell geometry. These characteristics will be important inputs to an electrochemical model for predicting performance of this electrochemical reactor.

To describe the CPBE, consider a vessel inclined by an angle θ from the vertical, filled with solid particles. Suppose fluid is injected at the base of the vessel through a distributor. At low flow rate, the liquid simply moves up without disturbing the particles, and the pressure drop rises with increasing flow rate. Upon reaching a certain flow rate, the particles begin to move. If the fluid flow rate is high enough, the liquid velocity causes a stream of particles to rise rapidly in a continuous sheet of particles near the upper wall of the vessel. When these particles reach the top the action of gravity causes them to spill down, moving downwards as an expanded packed bed. The combined particle motion results in a circulation of particles (Fig. 1). The overall circulating bed becomes a combination of a dilute phase of upward moving solids entrained with a co-current flow of fluid, and a dense phase of downward moving particles with counter-current percolation of fluid. A systematic cyclic pattern of solid particles circulation is thus established giving rise to a unique hydrodynamic system. The dilute phase is called the 'rising layer' while the dense phase is referred to as the 'descending layer' (Fig. 2(a)). The particles travel along the path, and so circulate through the rising and descending layers. Experimental observation revealed that particles do not cross from lean to dense phase except at the ends of the bed.

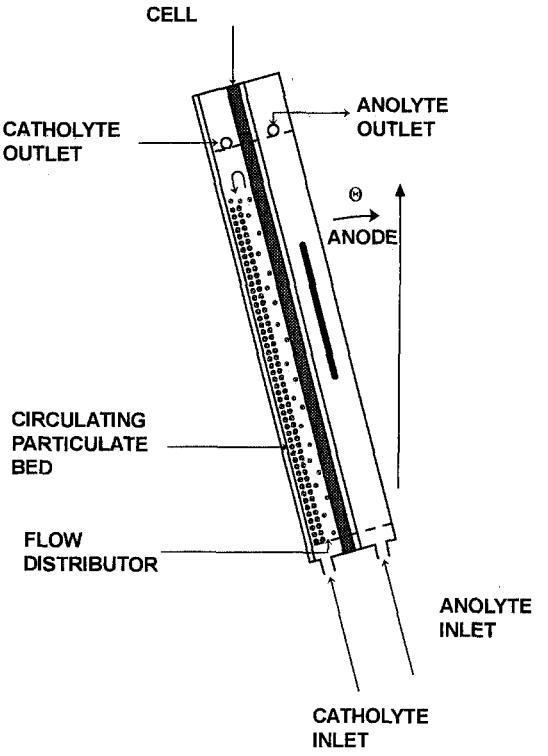

Fig. 1. A schematic of the experimental particulate bed electrode cell used in this study. Only the cathode was studied here; the anode chamber and anolyte flow was not used in these studies.

2. Model approach and description

Hydrodynamic studies of moving particle systems in gas–solid systems have been proposed in literature. Generally, the models follow one of the two schools of thought; a dilute upward moving gas–solid suspension surrounded by a denser annulus of downward flowing solids (core-annulus models) [14–17] or packets of upward and downward moving solids occupying a dilute continuum of discrete particles (cluster models) [18–25]. The CPBE under investigation is composed of two distinct and easily identifiable regions (Fig. 2(a)); a dilute upward moving (co-current) liquid–solid layer (rising layer) and a dense downward moving (counter-current) solid layer (descending layer) in a situation similar to the core-annular system in the spouted beds. The two layers can be treated as separate systems. The inlet region was not examined in the model because it involves unknown interactions, so the model may not apply to very short beds.

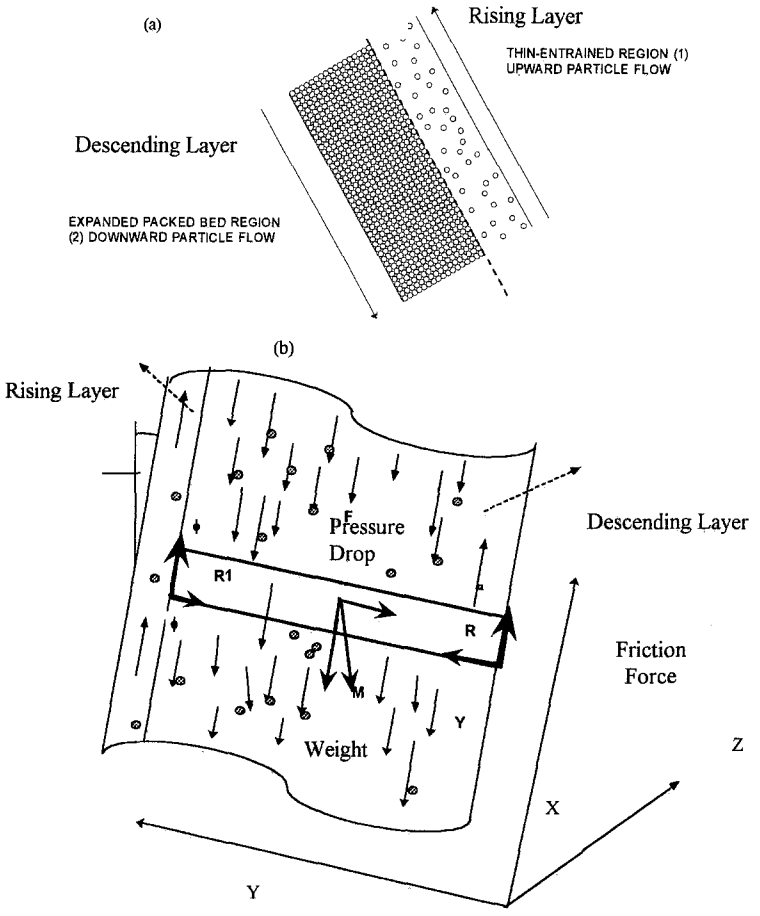

Fig. 2. (a) The CPBE contains two distinct and easily identifiable regions, the rising layer and the descending layer; (b) cross section in the CPBE showing forces on a volume element.

2.1. *Rising layer*

The rising layer is a continuous sheet of rising solid particles and liquid. The thickness can vary from a few millimetres to over 5 mm (total bed thickness is on order of 25 mm) which occupy about 5–20% of the total bed (the thickness depends on the tilt angle, solution viscosity and particle size). As the fluid passes upward through the bed, a pressure gradient is established through the length of the bed while the individual particles separate from each other. The total pressure drop along the bed can therefore be obtained by integrating the longitudinal pressure gradient profile from bottom to top.

Comparing various solid–liquid hydrodynamic systems, an entrained fluidized bed hydrodynamic behaviour is a system most appropriate for the description of the rising-layer velocity inside the CPBE bed. The pressure gradient in the rising layer is given by the following equation [26]:

$$\Delta P_R = -(\rho_s - \rho_f)(1 - \epsilon_R) g H_R \cos\theta \qquad (1)$$

In general, liquid fluidized systems are characterized by regular bed expansion, that is, the velocity increases from the minimum fluidization velocity to the terminal falling velocity of the particles, or

$$U_l / U_i = \epsilon_R^n \qquad (2)$$

where U_l is the superficial liquid velocity, U_i is a function of the terminal velocity [26] as shown in Equation 3, n is the Richardson and Zaki index [27, 28] and ϵ_R is the fluidized bed porosity.

The velocity U_i is related to the terminal velocity by

$$\log U_i = \log U_t - d_p/D \qquad (3)$$

Here, d_p is the mean diameter of bed particles and D is the mean hydraulic diameter of the rising layer.

Equation 2 applies to fluidized beds (no net motion of solids exists). To describe the motion occurring in the rising layer in the circulating bed, the equation requires modifications as follows:

$$V_l = U_l / \epsilon_R \qquad (4)$$

where V_l is the relative interstitial velocity in the rising layer.

Having obtained the value of V_l, it is possible to relate the liquid and solid velocities in the rising layer. The basis of the Wallis drift-flux [29] model which focuses on the relative motion rather than the motion of individual phases, can be used to relate the velocities. The drift flux model relates the interstitial phase velocities between the solid and the liquid in the rising layer (the liquid rising layer velocity and the solid rising layer velocity are in the same direction). This is shown by the following equation:

$$V_l = V_{LR} - V_{SR} \qquad (5)$$

Also, the phase velocities are related to the superficial phase velocities as follows

$$V_{LR} = \frac{U_{LR}}{\epsilon_R} \tag{6}$$

$$V_{SR} = \frac{U_{SR}}{1 - \epsilon_R} \tag{7}$$

The terminal velocity can be estimated as [26]

$$U_t = \left(\frac{4d_p(\rho_s - \rho_f)g}{3\rho_f C_D}\right)^{\frac{1}{2}} \tag{8}$$

Combining Equations 2 to 8, leads to

$$U_{LR}(1 - \epsilon_R) - U_{SR}\epsilon_R = \left(\frac{4d_p(\rho_s - \rho_f)g}{3\rho_f C_D}\right)^{\frac{1}{2}} e^{-d_p/D}\epsilon_R(1 - \epsilon_R) \tag{9}$$

Equation 9 is useful since it is possible to use physical data such as solid and liquid densities and rising layer voidage together with the particle size to describe the relationship between liquid and solid velocities in the rising layer.

2.2. *Descending layer*

The descending layer is a slightly expanded packed bed. This part of the bed occupies the majority of the cell (70–90%). The Ergun equation is a satisfactory generalized relation for relating pressure drop to flow rate through fixed beds. The Ergun equation can be corrected for the particles shape by introducing a sphericity parameter. The particles employed in this study were spherical and within a narrow diameter range (d_p = 420–550 μm). For a wide range of particle diameters, the Ergun equation can be still employed by using the mean average particle diameters. The Ergun equation can be used to predict the pressure drop as long as no gas evolution takes place. A recent study by Wragg *et al.* [30] suggests a correction for the coefficient in the first term as a result of gas evolution. The correction is a function of current density (i.e., gas evolution rate).

The Ergun equation is written as [31]

$$-\frac{dp}{dx} = \frac{150(1 - \epsilon_D)^2\mu_f V_2}{d_p^2\epsilon_D^3} + \frac{1.75(1 - \epsilon_D)\rho_f V_2^2}{d_p\epsilon_D^3} \tag{10}$$

where V_2 represents the slip velocity in the descending layer. Having obtained the value of V_2 it is possible to relate the liquid and solid phase velocities in the descending layer:

$$V_2 = V_{LD} - V_{SD} \tag{11}$$

The pressure drop in the packed bed can be related to the force balance around a small element inside the bed. In this region, there are several forces in action which lead to a stable system. These forces are present due to the weight of the bed, to the relative motion of the liquid and solid particles, and to friction forces between the bed back plate and friction between descending–rising layers. A section of circulating bed is shown in Fig. 2(b) with the forces depicted. The force balance in the x-direction can be written in terms of the 'pressure drop', 'frictional force' and 'weight' as follows:

$$[-\Delta P A_D] + [\tan\phi RWH_D] - [(\rho_s - \rho_f)(1 - \epsilon_D)(g\Delta x(A_D)\cos\theta] = 0.0 \tag{12a}$$

The force balance in the y-direction can be written in terms of the 'reaction' and 'weight' forces as follows:

$$(RWH_D) - [(\rho_s - \rho_f)(1 - \epsilon_D)(g\Delta x A_D \sin\theta)] = 0.0 \tag{12b}$$

Combining force balance (Equation 12(a) and (b)) in x- and y-directions gives:

$$\frac{dP}{dx} = (\rho_s - \rho_f)(1 - \epsilon_D)g(\tan\phi\sin\theta - \cos\theta) \tag{12c}$$

$$\nabla P = (\rho_s - \rho_f)(1 - \epsilon_D)g(\tan\phi\sin\theta - \cos\theta)H_D \tag{12d}$$

This equation can be used to find the pressure drop in the descending layer in the CPBE as a function of several parameters.

The pressure drop calculated from the Ergun equation should be equal to the pressure drop calculated from the force balance, thus Equation 10 and Equation 12(c) are equated to give

$$-(\rho_s - \rho_f)(1 - \epsilon_D)g(\tan\phi\sin\theta - \cos\theta) = \frac{150(1 - \epsilon_D)^2\mu_f V_2}{d_p^2\epsilon_D^3} + \frac{1.75(1 - \epsilon_D)\rho_f V_2^2}{d_p\epsilon_D^3} \tag{13}$$

Solving with respect to V_2 gives

$$V_2 = -\frac{42.86\mu_f(1 - \epsilon_D)}{d_p\rho_f} + \left[\left(\frac{42.86\mu_p(1 - \epsilon_D)}{d_p\rho_f}\right)^2 - \frac{d_p^2\epsilon_D^3(\rho_s - \rho_f)(\tan\phi\sin\theta - \cos\theta}{1.75(1 - \epsilon_D)\rho_f}\right]^{1/2} \tag{14}$$

Having obtained this value of V_2 which represents the slip velocity in the descending layer, it is possible to relate the liquid and solid phase velocities in the descending layer (Equation 11).

The slip velocity reflects the interaction between liquid and solids and is an essential parameter for the process modelling. Equation 5 and 14 represent the slip velocity in the rising and descending layer, respectively. Slip velocity is a main factor influencing mass transfer, momentum transfer and electrochemical reaction. So the prediction and/or measurement of the slip velocity is important to obtaining an in-depth understanding of liquid–solid two phase flow.

2.3. *Particle motion at interface*

In the rising layer, the liquid velocity is greater than the solid particle velocity because the solid particles settle with respect to the liquid (under the effect of the gravity). As a result, gravity will force particles to move towards the descending layer as is shown in Fig. 3. Thus, the solid particles in the rising layer

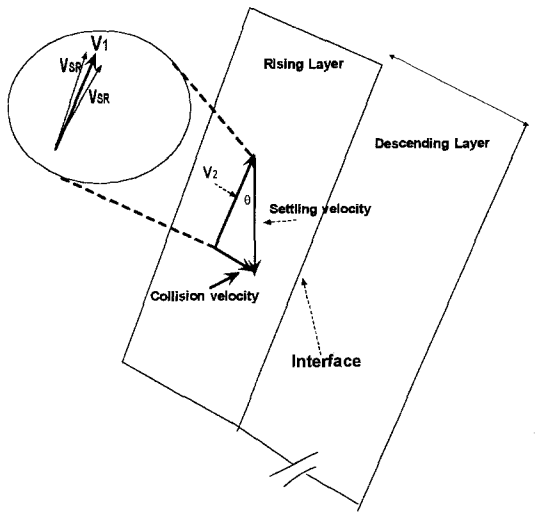

Fig. 3. Particles motion at the interface and velocity vectors.

collide with the descending layer and bounce off the descending layer and proceed up the rising layer in a series of bouncing steps. The collision velocity depends on the solid velocity in the rising layer, while the velocity at which the solid particles will return back to the rising layer is proportional to the difference between the solid velocity in the descending layer and in the rising layer.

By assuming the solid velocity in the descending layer is negligible with respect to the solid velocity in the rising layer, equating these two velocities at the interface by inserting the proportionality constant C gives the following equation

$$V_{LR} - V_{SR} = \frac{C}{\tan\theta} \times V_{SR} \tag{15}$$

where C is the proportionality constant (different values for C were tried, $C = 0.01$ was found to be the most appropriate value to fit the data). This is tantamount to saying the difference between the V_{LR} and V_{SR} is small as was observed experimentally. Also, the proportionality to V_{SR} becomes smaller as the angle θ increases.

2.4. *Mass balance*

Since no solids leave the bed, the solid flow rate in the rising layer has to equal the solid flow in the descending layer as follows:

$$G_{SD} = -G_{SR} \tag{16}$$

Thus,

$$V_{SD}(1 - \epsilon_D)\rho_s A_D = -V_{SR}(1 - \epsilon_R)A_R\rho_s \tag{17}$$

Solving for velocity in the rising layer gives

$$V_{SR} = -\frac{V_{SD}(1 - \epsilon_D)A_D}{(1 - \epsilon_R)A_R} \tag{18}$$

Having obtained the solid velocity and the rising layer thickness inside the bed, it is possible to calculate the solid circulation rate (CR) inside the bed as follows:

$$CR = V_{SR}(1 - \epsilon_R)Wt_R \tag{19}$$

where t_R represents the rising layer thickness.

The total inlet liquid flow will pass through both the rising and the descending layers. If the inlet mass flow rate is $Q\rho_f$, then

$$Q\rho_f = G_{LD} + G_{LR} \tag{20}$$

$$Q = V_{LD}\epsilon_D A_D + V_{LR}\epsilon_R A_R \tag{21}$$

This equation relates the inlet volumetric flow rate with the liquid descending layer velocity, liquid velocity in the rising layer, and to the rising and descending layer thickness through A_R and A_D, respectively. The total thickness of the bed is represented as the summation of the descending and the rising layer thickness as ($T = t_R + t_D$). By solving Equation 21, it is possible to predict the rising layer thickness for different design and operating parameters.

2.5. *Particle number balance*

The total number of particles inside the bed is constant, assuming no particles leave the bed:

$$(1 - \epsilon_D)t_D H_D + (1 - \epsilon_R)t_R H_R = (1 - \epsilon_I(t_R + t_D)H_0 \tag{22}$$

where ϵ_D, ϵ_R and ϵ_I are descending layer, rising layer, and initial bed voidages, respectively, and H_0 is the initial collapsed height. Upon knowing the rising layer thickness and rising layer voidage, Equation 22 can be used to calculate the descending layer voidage.

2.6. *Voidage distributions*

One of the most important characteristics of any particulate bed is its voidage, which is defined as the fraction of the total volume which is made up of the free space between the particles, and filled with fluid. The solid phase in the descending layer is assumed to be similar to the annulus in the case of the spouted bed which is essentially a loose packed bed [32, 33]. The voidage in this region is substantially constant and equal to that in a fixed bed of loosely packed particles. Indeed, slight differences of voidage in different parts of the descending layer can frequently be observed. The fraction voidage (ϵ_D) in a packed bed is related to the particle sphericity [26]. Voidage of a randomly packed bed of uniformly sized particles increases as particles become less spherical.

The rising layer is similar to a riser through which the particles are being transported in a dilute phase. The rising layer voidage is higher just above the distributor than along the height of the bed. For a *stable* system in equilibrium, the pressure drop along the bed should be uniform across the descending and rising layers. Thus, by setting equality between Equation 1 and Equation 12(d), this yields

$$-(\rho_s - \rho_f)(1 - \epsilon_R)gH_R\cos\theta = (\rho_s - \rho_f)(1 - \epsilon_D)g(\tan\phi\sin\theta - \cos\theta)H_D \tag{23}$$

Rearranging the above equation gives

$$\epsilon_R = 1 + [(1 - \epsilon_D)(\tan\phi\tan\theta - 1)] \times \frac{H_D}{H_R} \tag{24}$$

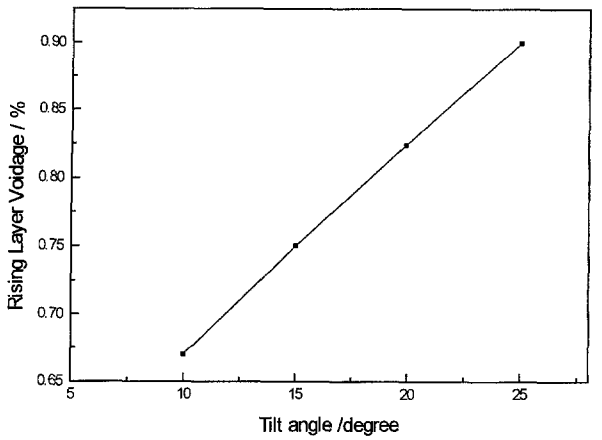

Fig. 4. Effect of cell tilt angle on the rising layer voidage.

The rising layer voidage depends on the descending layer voidage, the cell tilt angle and the friction coefficient. As the cell tilt angle increases the rising voidage increases. Fig. 4 shows this effect clearly.

3. Results

3.1. *Independent variables and calculation algorithm*

The input variables or independent parameters to the model include properties of the cell, the liquid and the particles which all can be evaluated independently. The input variables are summarized in Table 1. Table 2 is a summary of the algorithm to solve the mathematical relationships which describe the fluid and particle behaviour in a CPBE.

3.2. *Model validation and simulation results*

To determine the validity of the proposed model, comparisons are made between the simulated and experimental observation to illustrate the ability of the model to predict the effect on dependent parameters, such as pressure drop and layer thickness of operating parameters such as the superficial liquid velocity, particle diameter and density. The fluid in all experiments was water. (Details of the experiments can be found in [34].) Figures 5 and 6 show the rising layer thickness predicted from the model as compared

Table 1. Values used for independent parameters of model for CPBE system

Independent parameter	*Symbol*	*Values used*
Particle diameter	d_p	420–550 μm
Solution viscosity	μ_f	0.01 poise
Solution density	ρ_f	10^3 kg m^{-3}
Particle density	ρ_s	8.6–11.4 $\times$ 10^3 kg m^{-3}
Solution flow rate	Q	30–130 $\times$ 10^{-6} m^3 s^{-1}
Width of the bed	W	14 $\times$ 10^{-2} m
Bed thickness	T	2.54 $\times$ 10^{-2} m
Cell tilt angle	θ	0–25° (degree from vertical)
Rising bed height/descending bed height	H_R/H_D	1.2
Initial height of the bed	H_0	20 $\times$ 10^{-2} m

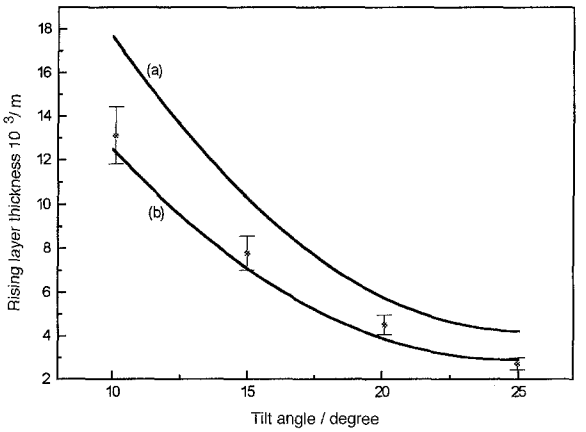

Fig. 5. Comparison between the experimental and the predicted rising layer thickness for copper particles. Flow rate 100 cm^3 s^{-1}. Model prediction: (a) 250 μm and (b) 500 μm. (*) Experimental findings. Equivalent diam. 500 μm.

with the experimental measurements made with copper and titanium particles respectively. Examination of Figs 5 and 6 indicates a reasonably good agreement between the simulated and experimental measured values. There are some differences which may be due to the model assumption that all particles are of uniform diameter, while the actual experiments were done with particles with a distribution of particle diameters.

To measure the descending layer particle velocity, approximately 50 of the copper particles were marked by paint. These particles, along with the unmarked particles were placed in the cell. Descending layer velocity was measured by recording the time needed for the tagged particle to travel a certain distance (15 cm distance between two marked lines along the bed). The velocity for a number of particles were measured at various positions across the bed, the average of all particle velocities are reported in Fig. 7 along with error bars depicting the standard deviation of measured velocity.

A comparison of the calculated and measured descending layer velocities are given in Fig. 7. This figure shows that the predicted velocities from the model agree reasonably well to experimentally measured

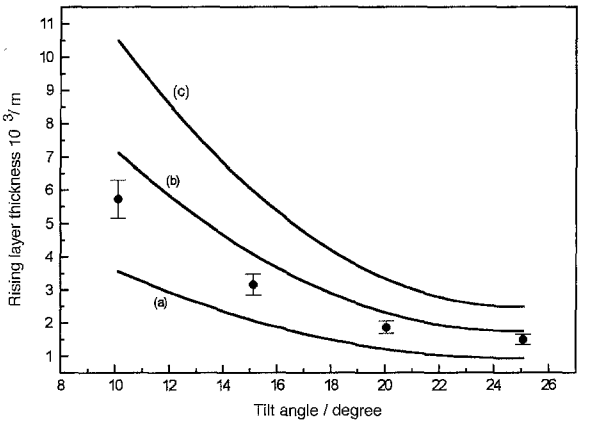

Fig. 6. Comparison between the experimental and the predicted rising layer thickness for titanium particles (experimental error 5–8%). Flow rate 10^{-4} m^3 s^{-1}. Model prediction: (a) d_p = 750 μm, (b) d_p = 1400 μm, (c) d_p = 500 μm. (●) Experimental findings chopped wire, d_p = 1400 μm.

Table 2. Algorithm of the mathematical relationships and methods of solution to describe the fluid and particle behaviour in the CPBE

Calculation of the slip velocity in the descending layer
assume descending layer voidage, ϵ_D, is constant

$$V_2 = -\frac{42.86\mu_f(1-\epsilon_D)}{d_p\rho_f} + \left(\left(\frac{42.86\mu_f(1-\epsilon_D)}{d_p\rho_f}\right)^2 - \frac{d_p^2\epsilon_D^3(\rho_s-\rho_f(\tan\phi\sin\theta-\cos\theta)}{1.75(1-\epsilon_D)\rho_f}\right)^{1/2}$$

↓

Calculation of the voidage in the rising layer

$$\epsilon_R = 1 + ((1-\epsilon_D)(\tan\phi\tan\theta - 1)) \times \frac{H_D}{H_R}$$

Calculation of the terminal velocity U_t

$$U_t = \left(\frac{4d_p(\rho_s-\rho_f)g}{3\rho_f C_D}\right)^{1/2}$$

Calculation of U_i

$$\log U_i = \log U_t - d_p/D$$

assume rising layer thickness (where D, hydraulic radius, is a function of rising layer thickness

Calculation of the slip velocity in the rising layer

$$\frac{U_l}{U_i} = \epsilon_R^n$$

$$V_l = \frac{U_l}{\epsilon_R}$$

Calculation of the particles velocity in the rising layer

$$V_l = V_{LR} - V_{SR}$$

$$(V_{LR} - V_{SR})\tan\theta = C\ V_{SR}$$

↓

Calculation of the liquid velocity in the rising layer

$$V_{LR} = V_l + V_{SR}$$

↓

Calculation of the thickness of the rising layer.

$$Q = (V_2 + V_{SD})\epsilon_D A_D + V_{LR}\epsilon_R A_R$$

A_R is a function of rising layer thickness

↓

Calculation of the particles velocity in the descending layer

$$V_{SR} = -\frac{V_{SD}(1-\epsilon_D)A_D}{(1-\epsilon_R)A_R}$$

Calculation of the liquid velocity in the descending layer

$$V_{LD} = V_2 + V_{SD}$$

↓

Particles number balance, calculate the descending layer voidage, if $\epsilon_{(calculated)} \cong \epsilon_{(assumed)}$ is ok
otherwise *correct* for the descending layer voidage

values. We also observed that particles movement in the rising layer are at velocities significantly greater than particles movements in the descending layer (perhaps by one to two orders of magnitude). This is in agreement with our calculation results.

In general, the model predictions qualitatively compare favourably to experimental observations during bed operation. These include rising layer and descending layer bed voidages, liquid flow distribution, and solid velocities. To more fully appreciate the impact of the independent parameters on bed characteristics, and ultimately electrochemical performance, model calculation studies were performed. Some of these are described in the following Section.

3.3. *Calculated behaviour of the model*

As a starting point typical values of the input parameters are inserted into the model. Table 3 summarize the effect of an *increase* of each independent variable on the characteristics (dependent variables) of the bed. A positive notation means that there is a tendency for the value of the property to increase. In the case of the descent rate of particles, V_{SD}, a positive sign denotes that the particles tend to descend faster.

Table 4 shows the necessary change in each of the independent variables which is required to effect an increase in the particle descent rate and the particle circulation rate, i.e. for a more stable bed operation. Since the rising layer is nearest the counter electrode,

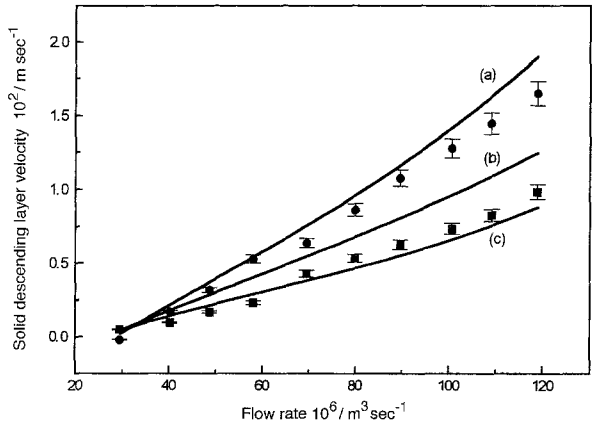

Fig. 7. Comparison between the experimental and predicted descending layer particle velocity inside the CPBE at different cell tilt angles (experimental error 5–8%). Model prediction for copper particles, $d_p = 550\,\mu$m. Tilt angle: (a) 15°, (b) 20° and (c) 25°. Experimental findings: (●) 20° and (■) 25°.

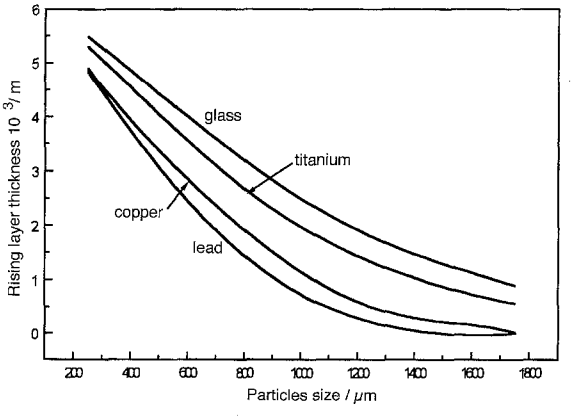

Fig. 8. Calculated rising layer thickness as a function of particle diameter for different particle densities (glass, titanium, copper and lead). Flow rate 10^{-4} m^3 s^{-1}. CPBE angle = 20°.

Table 3. Effect of increasing each input independent variable on the dependent characteristics

Independent parameters ↓	*Dependent characteristics*							
	Rising layer voidage	*Rising layer thickness*	*Solid velocity in descending layer*	*Liquid velocity in descending layer*	*Solid velocity in rising layer*	*Liquid velocity in rising layer*	*Circulation rate*	*Pressure drop*
Tilt angle	Positive	Negative	Negative	Positive	Positive	Positive	Negative	Negative
Bed thickness	No effect	Negative	Negative	Positive	Negative	Negative	Negative	No effect
Friction coefficient	No effect	Negative	Negative	Positive	Positive	Positive	Negative	Negative
Solid density	No effect	Negative	Negative	Positive	Positive	Positive	Negative	Positive
Particle diameter	No effect	Negative	Negative	Positive	Positive	Positive	Negative	No effect
Solution density	No effect	Positive	Positive	Negative	Negative	Negative	Positive	Positive
Solution viscosity	No effect	Positive	Positive	Negative	Positive	Negative	Positive	No effect
Solution flow rate	No effect	Positive	Positive	Negative	Positive	Positive	Positive	Positive

Positive: Increasing the input variable increases the parameter value.
Negative: Increasing the input variable decreases the parameter value.
No effect: The input variable has no effect on the parameter.

this zone is particularly important for electrochemical cell performance. Therefore, it may be worthwhile to examine this region more carefully.

The model demonstrates that the rising layer thickness is a function of all independent parameters, in particular particle size, flow rate, particle density and the cell tilt angle. Rising layer thickness was calculated for different particle materials (i.e., different particle densities) including, lead, titanium, glass and copper (Fig. 8), as a function of particle size. The smaller the particle diameter, the larger the rising layer thickness. An increase of the particle density leads to a decrease of the rising layer thickness. The angle has a significant effect on the rising layer thickness; a cell tilt angle increase causes the rising layer thickness to decrease. Figure 9 shows the effect of particle size on the thickness of the rising layer for different cell tilt angles. Increasing solution flow rate and solution viscosity increases the rising layer thickness as shown in Figs 10 and 11.

The calculated liquid velocity in the rising layer is at least one order of magnitude more than the liquid velocity in the descending layer (Fig. 12). To experimentally examine the flow distribution, a dye tracer study was performed. In this experiment, a small volume (10 cm^3) of red ink was injected (to simulate a pulse input) at the cell inlet. The dye tracer indicated that fluid travelled upward in both descending and rising layers. Although it was difficult to measure or estimate the liquid velocity in the two layers, it was clear that the velocity in the rising layer was substantially greater than the upward liquid velocity in the descending layer.

Table 4. Objectives for stable bed circulation rate in the CPBE

Must decrease	*Must increase*
Tilt angle	Fluid viscosity
Angle of friction	Fluid density
Particle density	Flow rate
Particle size	
Thickness of bed	

4. Summary and conclusions

The particle and fluid dynamics of a circulation particulate bed electrode cell (CPBE) were the subjects of this research. Experiments demonstrated that the fluid and particle dynamics of the liquid–solid particle bed are a function of several parameters such as particle size, particle density, solution flow rate and cell tilt angle. Observation showed that as the fluid flow rate

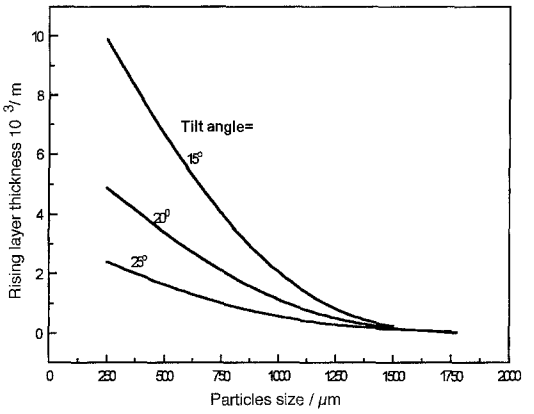

Fig. 9. Calculated rising layer thickness for copper particles as a function of particles diameter at three different tilt angles. Flow rate 10^{-4} m^3 s^{-1}.

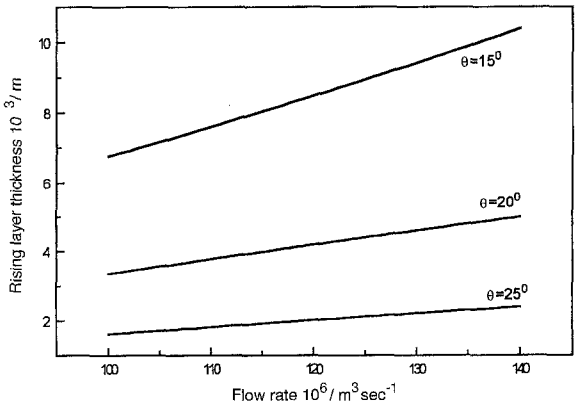

Fig. 10. Calculated effect of flow rate on the rising layer thickness for copper particles at three different cell tilt angles. Particle diam., $d_p = 500\,\mu m$.

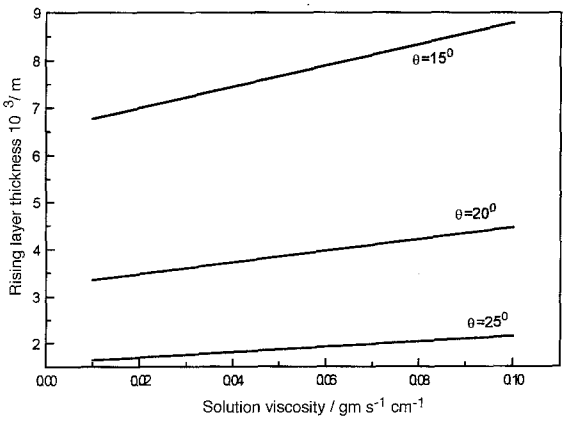

Fig. 11. Calculated effect of solution viscosity on the rising layer thickness for copper particles at different cell tilt angles. Particle diam., $d_p = 350\,\mu$m. Flow rate 10^{-4} m^3 s^{-1}.

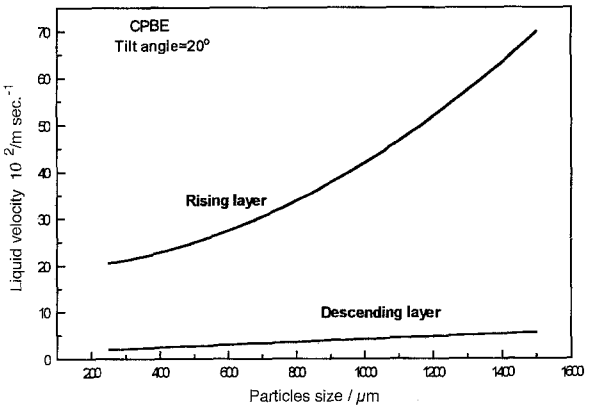

Fig. 12. Calculated comparison between liquid velocity in the descending layer and the rising layer as a function of copper particle diameter (tilt angle = 20°). Particle diam., $d_p = 500\,\mu$m.

increases, the bed expands and begins to divide perpendicular to the flow direction into two distinct dynamic regions. The first region is the rising layer, which is characterized by a narrow zone of particles moving upward with the fluid flow. The volume fraction of the particles in this zone is dilute (10–30%). As the particles reach the top of the bed, the action of the gravity causes them to spill to the downward moving packed bed region of the cell thus forming the second region, the descending layer. This region is a slightly expanded packed bed and it occupies the majority of the bed (particle volume (70–90%)). When the particles reach the bottom of the cell they re-enter the rising layer.

The pressure drop has been used to define the relative interstitial velocity in the descending layer. The rising layer is assumed to behave as an entrained bed, while the descending bed is assumed to be an expanded packed bed. Force balances, particle number and mass balances were used to complete the mathematical description.

The validity of the proposed model was demonstrated qualitatively by comparing the prediction of the rising layer thickness and downward particle velocity with data obtained for an experimental CPBE unit. Generally, the simulated results compared favourably with the experimental results. These model and experimental studies will serve as a basis for the prediction of the electrochemical performance (i.e., rising layer thickness as an indication of the active layer in the bed) of the CPBE cell. The model is also in qualitative agreement with a number of observations made during cell operation such as distribution of particles and solution flow rate.

Acknowledgements

Financial support for this research was provided by Faraday Technology Inc. and the US Advanced Research Projects Agency (ARPA) contract number MDA 972-93-C-0036. We are grateful to professor D. Feke for his many suggestions and guidance. B.D. is thankful to Jordan University of Science and Technology for the scholarship award.

References

[1] K. B. Mathur and N. Epstein, 'Spouted Beds', Academic Press, New York (1974).
[2] F. Goodridge, C. J. King and A. R. Wright, *Electrochim. Acta* **22** (1977) 1087.
[3] J. R. Backhurst, J. M. Coulson, F. Goodridge and R. E. Plimley, *J. Electrochem. Soc.* **116** (1969) 1600.
[4] F. Coeuret, *J. Appl. Electrochem.* **10** (1980) 687.
[5] H. D. Steppke and R. Kammel, *Erzmetall. Bd.*, 'Electrolysis with Fluidized Bed Electrodes', 26 H11 (1973) 533.
[6] G. S. James, B. I. Dewar and W. R. Moergeli, *US Patent 3 981 787* (1976).
[7] G. S. James, B. I. Dewar and W. R. Moergeli, *US Patent 3 945 892* (1976).
[8] A. F. R. Newton, *US Patent 4 065 375* (1977).
[9] J. A. E. Wilkinson, R. S. H. Leslie, D. M. Glindon, K. P. Haines and K. Baker, *US Patent 4 035 278* (1977).
[10] R. Kammel and H. W. Lieber, *Galvanotechnik* **69** (1978) 687.
[11] F. Goodridge, *Electrochim. Acta* **22** (1977) 929.
[12] F. Goodridge and C. J. Vance, *Electrochim. Acta* **22** (1977) 1073.
[13] K. Scott, *J. Appl. Electrochem.* **18** (1988) 504.
[14] K. Nakamura and C. E. Capes, *Can. J. Chem. Eng.* **51** (1973) 39.
[15] S. Morooka, K. Kawazuishi and Y. Yayo, *Powder Tech.* **26** (1980) 75.
[16] S. Morooka and K. Leschonski, *J. Chem. Eng.* **36** (1987) 59.
[17] F. Berruti and N. Kalogerakis, *Can. J. Chem. Eng.* **67** (1989) 1010.
[18] M. J. Rhodes, *Power Technol.* **60** (1990) 27.
[19] H. Arastoopour and D. Gidapow, *Ind. Eng. Chem. Fund.* **18** (1979) 123.
[20] Y. Li and M. Kwauk, *in* 'Fluidization' (edited by J. R. Grace and J. M. Matsen), Plenum Press, New York (1980), p. 537.
[21] B. Dinrong, J. Yong and Y. Zhiqing, *in* 'Fluidization' (edited by M. Kwauk and D. Kunii), Science Press, Beijing, China (1988), p. 155.
[22] M. Horio, K. Morishita, O. Tachibana and N. Murata, *in* 'Circulating Fluidized Bed Technology II', (edited by P. Basu and J. F. Large), Pergamon Press, Toronto (1988), p. 147.
[23] H. Ishii, T. Nakajima and M. Horio, *Jap. J. Chem. Eng.* **22**(5) (1989) 484.
[24] M. Horio and Y. Takei, *in* Proceedings of the 3rd International Conference on Circulating Fluidized Beds, 15 Oct., Nagoya, Japan (1990).
[25] H. Zhang, Y. Xie, Y. Chen and M. Hasatani, *in* Proceedings of the 3rd Conference on Circulating Fluidized Beds, 15 Oct., Nagoya, Japan (1990).
[26] D. Kunii and O. Kevenspiel, 'Fluidization Engineering', 2nd edn, J. Wiley & Sons, New York (1991).
[27] W. K. Lewis, E. R. Gilliland and W. C. Bauer, *Ind. Eng. Chem.* **41** (1949) 1104.
[28] A. Richardson and W. N. Zaki, *Trans. Inst. Chem. Eng.* **32** (1954).

[29] G. B. Wallis, 'One Dimensional Two Phase Flow', McGraw-Hill, New York (1967).
[30] V. D. Stankovic, G. Lazarevic and A. A. Wragg, *J. Appl. Electrochem.* **25** (1995) 864.
[31] S. Ergun, *Chem. Eng. Progr.* **48** (1952) 89.
[32] N. Epstein, *Ind. Eng. Chem. Process.* **7** (1968) 158.
[33] J. M. Matsen, *Ind. Eng. Chem.* **7** (1969) 159.
[34] B. M. Dweik, MSc thesis, Case Western Reserve University, May (1995).